ЖЭТФ, 2001, том 120, вып. 1 (7), стр. 183–190

PHASE TRANSITIONS IN $La_{1-x}Ca_xMnO_{3-x/2}$ MANGANITES

I. O. Troyanchuk**, *S. V. Trukhanov

Institute of Solids and Semiconductor Physics
National Academy of Sciences of Belarus
220072, Minsk, Belarus

H. Szymczak**

Institute of Physics, Polish Academy of Sciences
02-668, Warsaw, Poland

J. Przewoznik

University of Mining and Metallurgy
30-059, Krakow, Poland

K. Bärner

IY Physikalishes Institut
D37073, Göttingen, Germany

Submitted 8 December 2000

The crystal structure parameters, magnetic and electrical properties of $La_{1-x}Ca_xMnO_{3-x/2}$ reduced manganites with $0 \le x \le 0.5$ are established. These investigations contribute to the understanding of magnetic interactions in manganites without Mn^{4+} ions. It is found that these manganites show a long-range antiferromagnetic order up to $x = 0.09$ and transform into spin glasses at $0.09 < x \le 0.35$. The compositions in the range $0.35 < x \le 0.5$ show a strong increase in the spontaneous magnetization and critical point associated with the appearance of spontaneous magnetization and can therefore be viewed as inhomogeneous ferromagnets. The magnetic and crystal structure peculiarities of $La_{0.5}Ca_{0.5}MnO_{2.75}$ are established by the neutron diffraction method. The strongly reduced samples show a large magnetoresistance below the point where the spontaneous magnetization develops. The magnetic phase diagram of $La_{1-x}Ca_xMnO_{3-x/2}$ is established by magnetization measurements. The magnetic behavior is interpreted assuming that the Mn^{3+}–O–Mn^{3+} magnetic interaction is anisotropic (positive–negative) in the orbitally ordered phase and isotropic (positive) in the orbitally disordered phase. The introduction of the oxygen vacancies changes the magnetic interaction sign from positive to negative, thereby leading to a spin glass state in strongly reduced compounds. The results obtained reveal unconventional features for strongly reduced manganites such as a large ferromagnetic component and high magnetic ordering temperature as well as a large magnetoresistance in spite of absence of Mn^{3+}–Mn^{4+} pairs. For the explanation of these results, the oxygen vacancies are supposed to be ordered.

PACS: 72.15.Gd, 75.30.Kz, 75.70.Pa

1. INTRODUCTION

The hole-doped $La^{3+}_{1-x}A^{2+}_x(Mn^{3+}_{1-x}Mn^{4+}_x)O_3$ perovskites, where A represents divalent alkaline-earth elements such as Ca, Sr, and Ba, have recently attracted much attention because of their unusual magnetic and transport properties [1, 2]. The parent compound $La^{3+}Mn^{3+}O_3$ is an antiferromagnetic insulator with the A-type magnetic order [3]. This compound contains Mn^{3+} ions with the $t^3_{2g}e^1_g$ ($S = 2$) electronic configuration surrounded by the oxygen octahedron. It is accepted that the t^3_{2g} and e^1_g electrons are localized and their total magnetic moment is determined only by the total spin because their orbital magnetic moment is frozen. It is known that Mn^{3+} is the Jahn–Teller ion with the higher energy e_g and the

*E-mail: troyan@ifttp.bas-net.by
**E-mail: szymh@ifpan.edu.pl

smaller energy t_{2g} electronic levels in the octahedral oxygen coordination. An orbital ordering is observed and the interaction of the magnetic moments of manganese is anisotropic as a result of the Jahn–Teller effect. The antiferromagnetic spin axis is directed almost along the b-axis and the ferromagnetic moment along the c-axis [4].

$La_{1-x}A_xMn^{3+}_{1-x}Mn^{4+}_xO_3$ exhibits a ferromagnetic ground state and a metal–insulator transition occurring near the Curie point at $x > 0.15$. In this case, Mn^{4+} ions are created from Mn^{3+}. The Mn^{4+} ion contains t^3_{2g} electrons only ($S = 3/2$). The interplay between the electrical transport and ferromagnetism in these systems is traditionally interpreted within the framework of double exchange interaction [5–7], where the magnetic coupling between Mn^{3+} and Mn^{4+} ions is considered to result from the motion of the e_g electron between two partially filled d shells with the strong Hund coupling on site.

However, the double exchange alone is not sufficient to explain all the properties of these compounds [8]. It has been shown that $A^{3+}_2Mn^{4+}_2O_7$ pyrochlores also exhibit a colossal magnetoresistance despite the absence of mixed manganese valence [9]. Recently, many compounds ($(La(Nd)_{1-x}Pb_xMnO_{3-x}F_x$, $La_{0.66}Ba_{0.34}Mn_{1-x}Nb_xO_3$, etc.) have been found and they show the ferromagnetic behavior and large magnetoresistance in spite of the absence of Mn^{4+} [10]. Goodenough [11] adduced arguments for the ferromagnetism to be due not only to the double exchange but also to the specific character of superexchange interactions in Mn^{3+}–O–Mn^{3+}, Mn^{3+}–O–Mn^{4+}, and Mn^{4+}–O–Mn^{4+} ion systems [11]. In the superexchange model, the ferromagnetic fraction of the exchange is determined by a virtual electron transfer from the half-filled e_g orbitals of the Mn^{3+} ion to the empty ones. Many recent experimental results have given evidence to the existence of a phase separation in manganites [12]. There is no general agreement concerning exchange interaction mechanisms in the hole-doped manganites. Despite numerous theoretical and experimental studies, the true nature of the colossal magnetoresistance in perovskites is still a matter of discussion.

Because Mn ions play a key role in electrical and magnetic properties of the manganites by providing charge carriers, magnetic moments, and local Jahn–Teller distortions, it is certainly worth investigating the properties of manganites containing only Mn^{3+} ions. The Mn^{3+}/Mn^{4+} ratio can be changed by various methods: (i) the substitution of Ln^{3+} ions by A^{2+} (Ca, Sr, Ba, Pb, and Cd) ions in the A sublattice of ABO_3 perovskite; (ii) the substitution of Mn ions by different transition elements (Cr, Fe, Co, etc.) in the B sublattice of perovskite, and (iii) the removal of oxygen ions, which produces a reduction process where Mn^{4+} ions are converted into Mn^{3+} and their coordination number decreases.

In this work, the third method is chosen to change the Mn^{3+}/Mn^{4+} ratio because there are not enough data on the results of its application. Moreover, very intriguing magnetic and magnetoresistance properties have been revealed for $La_{0.5}Ca_{0.5}MnO_{3-\gamma}$ [13] and $Ln_{0.5}Ba_{0.5}MnO_{3-\gamma}$ (Ln = Pr, Nd) [14, 15] systems in our previous investigations. It was shown that these compounds can exhibit both a large magnetoresistance and a ferromagnetic component. It is notable that the oxygen content in manganites can vary from 2.5 [16] to 3.27 [17]. A much smaller degree of the oxygen nonstoichiometry was found for $LaVO_{3+\gamma}$ ($0 \le \gamma \le 0.05$) and $LaTiO_{3+\gamma}$ ($0 \le \gamma \le 0.08$), while $LaCrO_3$ and $LaFeO_3$ do not perfectly reveal the deviation from the stoichiometry. This behavior may result from a much larger reduction in the ionic radius from Mn^{3+} to Mn^{4+} than it is found for other transition metal perovskites [18].

In this paper, we study the oxygen reduction effect on the magnetization and resistivity of Ca-doped manganites $La_{1-x}Ca_xMnO_{3-x/2}$ for $x \le 0.5$. These compounds have already been known at the very early stage of the experimental [3, 4, 19, 20] and theoretical [21, 22] studies of transition-metal oxides. The phase diagram of $La_{1-x}Ca_xMnO_3$ compounds with $0 \le x \le 1$ can be found elsewhere [23–26]. However, the phase diagram for $La_{1-x}Ca_xMnO_{3-x/2}$ series has not been proposed earlier. Our study shows that both magnetic and electric properties are very sensitive to the oxygen content variation.

2. EXPERIMENT

Polycrystalline $La_{1-x}Ca_xMnO_{3+\gamma}$ samples with $-0.03 \le \gamma \le 0.1$, $x = 0$, 0.05, 0.09, 0.12, 0.15, 0.18, 0.25, 0.30, 0.35, 0.40, 0.45, 0.50 were fabricated with conventional ceramic technology. La_2O_3, $CaCO_3$, and MnO_2 were mixed, compacted, and prefired at 1000°C for 2 h in air. The pellets were then again ground and synthesized at 1550°C during 2 h in air, which was followed by quenching the samples with a low concentration of Ca ions from 900°C and slowly cooling the samples with a high concentration of Ca ions at the rate of 80°C/h in order to obtain the stoichiometric oxygen content. The X-ray powder diffraction data were recorded at room temperature with the DRON-3 diffractometer in CoK_α radiation. According

to X-ray measurements, all the as-prepared samples were single-phase perovskites with the orthorhombic symmetry of the unit cell. The thermogravimetric study revealed the as-prepared samples in the range $0 \le x \le 0.18$ to have the oxygen content slightly above the stoichiometric value ($\gamma \le 0.1$). The excess of oxygen decreases gradually as the calcium content increases. The samples with $x = 0.25$, 0.30, 0.35 are stoichiometric ($\gamma \approx 0$). The samples with $x = 0.40$, 0.45, 0.50 have the oxygen content slightly less than the stoichiometric value ($\gamma \ge -0.03$). In order to prepare the stoichiometric samples, the compositions in the range $0 \le x \le 0.18$ were annealed in small evacuated silica tubes at 700°C during 30 h using metallic tantalum as an oxygen getter. The amount of Ta was calculated assuming that the final products are Ta_2O_5 and stoichiometric compositions $La_{1-x}Ca_xMnO_3$ according to the relation

$$La_{1-x}Ca_xMnO_{3+\gamma} + \frac{2\gamma}{5}Ta \rightarrow \rightarrow La_{1-x}Ca_xMnO_3 + \frac{\gamma}{5}Ta_2O_5. \quad (1)$$

In contrast, the samples with $x = 0.40$, 0.45, and 0.50 were annealed in air at 900°C during 48 h. These reactions can be described by

$$La_{1-x}Ca_xMnO_{3+\gamma} + \frac{|\gamma|}{2}O_2 \rightarrow La_{1-x}Ca_xMnO_3. \quad (2)$$

Polycrystalline $La_{1-x}Ca_xMnO_{3-x/2}$ samples with $x = 0$, 0.05, 0.09, 0.12, 0.15, 0.18, 0.25, 0.30, 0.35, 0.40, 0.45, 0.50 were obtained by the topotactic reduction method in the above-mentioned manner. The reduction of the samples was performed at 900°C during 2 h in small evacuated silica tubes in presence of metallic Ta. The final oxygen content was calculated from the change in the weight of samples during the reduction. The relative error in oxygen content measurements did not exceed 1%. Therefore, the chemical formula for the reduced samples can be written as $La_{1-x}Ca_xMnO_{3-x/2\pm0.02}$. The reoxidation process leads to an increase in the weight corresponding to the loss of the weight during the reduction. According to X-ray measurements, almost all the samples from the $La_{1-x}Ca_xMnO_{3-\gamma}$ series (with $\gamma = 0, x/2$) were single-phase perovskites with the O^1-orthorhombic ($x \le 0.09$) or O-orthorhombic ($0.12 \le x \le 0.50$) unit cells similar to the as-prepared ones.

Magnetic and electric measurements have been performed for compositions corresponding to both $La_{1-x}Ca_x(Mn^{3+}_{1-x}Mn^{4+}_x)O_3$ and $La_{1-x}Ca_xMn^{3+}O_{3-x/2}$ series. For the magnetic measurements, an OI-3001 vibrating sample magnetometer was used in the temperature range from 4 to 300 K. Resistivity measurements were performed using the standard four-probe method with ultrasonically deposited indium contacts. The dc-resistivity data were collected for well-sintered samples in the form of bars with $10 \times 2 \times 2$ mm dimensions over the temperature range from 77 to 350 K. The magnetoresistance MR was calculated using the formula

$$MR = \frac{\rho(H) - \rho(H=0)}{\rho(H=0)} \cdot 100\%, \quad (3)$$

$\rho(H)$ is the resistivity in the magnetic field of 9 kOe, and $\rho(H = 0)$ is the resistivity without the magnetic field.

Neutron diffraction measurements for the $La_{0.5}Ca_{0.5}MnO_{2.75}$ sample were performed in Berlin Neutron Scattering Center using the E2 Flat Cone diffractometer with the wavelength of neutrons $\lambda = 1.79635$ Å.

3. RESULTS AND DISCUSSION

The crystal structure parameters for both $La_{1-x}Ca_xMnO_3$ and $La_{1-x}Ca_xMnO_{3-x/2}$ series are displayed in Fig. 1. Both stoichiometry and reduced series exhibit orthorhombic distortions in the entire range of the calcium concentration, however O^1-orthorhombic distortions ($c/\sqrt{2} < a \le b$) transform into O-orthorhombic ones ($a < c/\sqrt{2} < b$) at $x \sim 0.1$. According to Goodenough, the O^1 distortions are caused by the orbital ordering, which is a result of the cooperative static Jahn–Teller distortions of Mn^{3+} in $LaMnO_3$. As a dopant ion concentration increases, the removal of cooperative Jahn–Teller distortions is observed [25]. The reduced compounds have only Mn^{3+} ions, however oxygen vacancies destabilize the parent orbital ordering, and therefore, the Jahn–Teller distortions. For the samples with $x < 0.1$, oxygen vacancies are insufficient in order to remove the cooperative Jahn–Teller distortions, and the unit cell of these samples has the O^1-orthorhombic symmetry. For both series, the volume of the unit cell decreases gradually as the calcium content increases. This is explained by the decrease in the size effect contribution to the crystal structure distortions. However, this process is much less pronounced for $La_{1-x}Ca_xMnO_{3-x/2}$ series. The appearance of vacancies leads to decreasing in the average oxidative state of manganese. It is well known that the ionic radius of Mn^{3+} is larger than that of Mn^{4+}. The effective ionic radii of Mn^{3+} and Mn^{4+} in the octahedral oxygen coordination are 0.645 Å and 0.530 Å, respectively [27]. The vacancies must therefore reduce the unit cell volume, whereas the

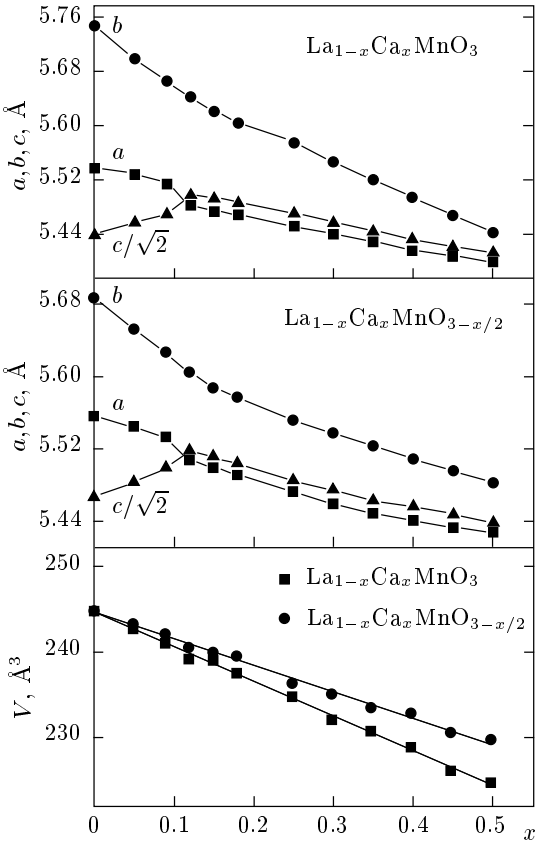

Fig. 1. The crystal structure parameters for $La_{1-x}Ca_xMnO_3$ stoichiometric (top panel) and $La_{1-x}Ca_xMnO_{3-x/2}$ reduced series (medium panel). The bottom panel displays the unit cell volume as a function of Ca concentration

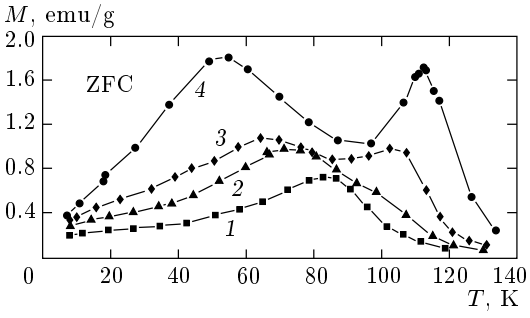

Fig. 2. ZFC magnetization versus temperature for samples with $x = 0.09$ (curve *1*), 0.12 (*2*), 0.15 (*3*), and 0.18 (*4*)

transformation of Mn^{4+} into Mn^{3+} must give rise to it. Our data indicate that the last process dominates.

The zero-field-cooled (ZFC) and field-cooled (FC) magnetizations in the field of 100 Oe for $La_{1-x}Ca_xMnO_{3-x/2}$ series are presented in Figs. 2 and 3. The samples in the ranges $0 \le x \le 0.12$ and $0.30 \le x \le 0.50$ show one ZFC-magnetization peak. The samples with $x = 0.15$, 0.18, 0.25 have two ZFC-magnetization peaks. The second magnetization peak at higher temperatures can be ascribed to a large magnetic anisotropy of these samples. The temperature corresponding to the largest magnetization on the $M(T)$ curve gradually decreases as the Ca concentration increases. We adopt two methods of estimating the critical temperature T_{cr} at which the magnetic transition occurs: (i) the onset of magnetic transition; T_{cr} is defined as the temperature point where ZFC and FC magnetizations become different in the field of 100 Oe; (ii) the completion of magnetic transition; T_{cr} is defined as the temperature point where the ZFC magnetization reaches its maximum value on the $M(T)$ curve measured in the field of 100 Oe. In the range $0 \le x \le 0.09$, these two temperatures are close to each other, which indicates a well-defined transition to the magnetically ordered state. The samples in the interval $0.12 \le x \le 0.18$ show an entirely different magnetic behavior. The ZFC magnetization for the sample with $x = 0.15$ demonstrates two peaks on the $M(T)$ curve, which implies a complex character of the magnetic ordering in this composition. The transition to the paramagnetic state remains narrow for all the compositions with $x \le 0.18$. For the $x = 0.30$ sample (Fig. 3), ZFC and FC magnetizations start to differ around 140 K, however a ZFC-magnetization peak is observed at a sufficiently low temperature 35 K. The ZFC-magnetization peak shifts towards high temperatures up to 160 K as the Ca concentration reaches $x = 0.50$.

In Figure 4, the magnetization is shown as a function of field at temperature of 6 K. It is difficult to estimate the spontaneous magnetization because for a majority of the reduced samples, the magnetization is not saturated in the field up to 1.6 T. The large slope in the $M(H)$ curve could be attributed to magnetic inhomogeneity or large magnetic anisotropy of these samples. The spontaneous magnetization first increases with increasing Ca content up to the $x = 0.15$ composition and then decreases. The largest spontaneous magnetization $M_s = 1.35\mu_B$ per formula unit (μ_B/f.u.) corresponds to the $x = 0.15$ composition, however even in this case, there is no pure ferromagnetic ordering because the expected value for the parallel ordering of all Mn^{3+} magnetic moments is around $4\mu_B$/f.u. The minimum spontaneous magnetization $M_s = 0.19\mu_B$/f.u. occurs for the $x = 0.30$ composition, where spin-glass properties are most pronounced. The surprise is that M_s rises again starting from the $x = 0.40$ composition and

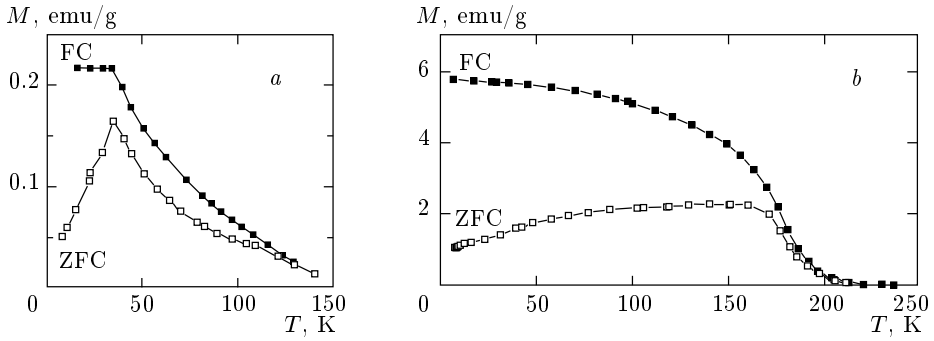

Fig. 3. ZFC and FC magnetizations versus temperature for (a) $x = 0.30$, (b) $x = 0.50$. $H = 100$ Oe

reaches $1.26\mu_B$/f.u. for the $x = 0.50$ composition.

For the $La_{0.5}Ca_{0.5}MnO_{2.75}$ sample, two neutron diffraction patterns were collected at 250 K (in the paramagnetic state) and 1.6 K to check the character of its magnetic ground state. The patterns were Rietveld refined with the two-phase model. In the refinements, the pattern profile was simulated by a split pseudo-Voigt function and the background was fitted to a seventh-degree polynomial function. The $La_{0.5}Ca_{0.5}MnO_{2.75}$ phase shows a clear asymmetric line broadening indicating the existence of large microstrains in this phase. The problem with the appropriate modeling of the (hkl)-dependent shape of the lines is the main source of difference between the measured pattern and fitted curve. The $La_{0.5}Ca_{0.5}MnO_{2.75}$ phase was fitted assuming orthorhombic $Pbnm$.

The most important structural parameters and agreement factors of the refinement are listed in table. The refined low-temperature value of the magnetic moment on the manganese atom is $\mu = 0.81(45)\mu_B$. The refined value of the Mn moment is not sensitive to the Mn spin direction.

According to electric resistivity measurements, all the reduced samples are semiconductors. The resistivity markedly increases as the temperature decreases (Fig. 5). There is no metal–insulator transition even for the $x = 0.15$ sample that shows the largest ferromagnetic component in the entire series. The magnetoresistance gradually increases below the point where the magnetic order develops. However, there is no magnetoresistance peak that was observed in the mixed-valence ferromagnetic manganites.

Summarizing our magnetization data, we constructed a hypothetic magnetic phase diagram of $La_{1-x}Ca_xMnO_{3-x/2}$ series (Fig. 6), i.e., a dependence of the magnetic transition temperature on the calcium concentration. The phase diagram of $La_{1-x}Ca_xMnO_3$

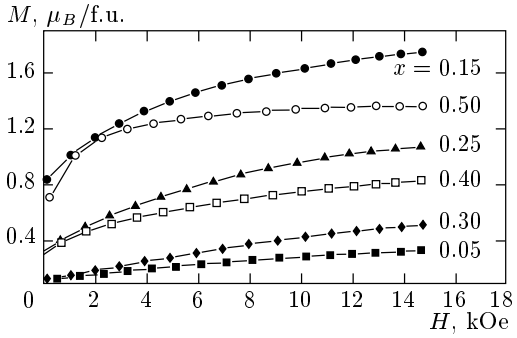

Fig. 4. The magnetization versus magnetic field curves for $La_{1-x}Ca_xMnO_{3-x/2}$ samples with $x = 0.05$, 0.15, 0.25, 0.30, 0.40, 0.50 measured at 6 K

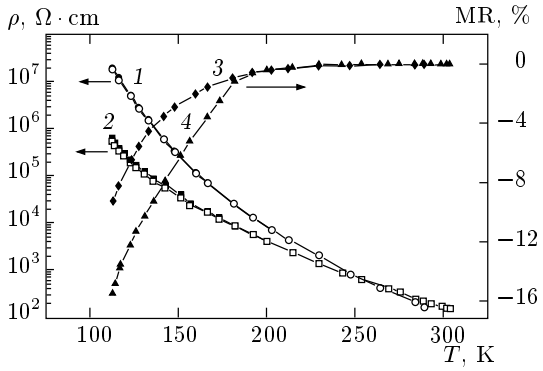

Fig. 5. The resistivity and magnetoresistance versus temperature for samples with $x = 0.15$ (curves *1* and *3*) and $x = 0.50$ (curves *2* and *4*)

compounds (with $0 \leq x \leq 1$) can be found elsewhere [23–26]. The $x = 0$ and $x = 1$ members of the $La_{1-x}Ca_xMnO_3$ system (namely, $LaMnO_3$ and $CaMnO_3$) are antiferromagnetic insulators at low temperatures, with the A- and G-type of magnetic ordering, respectively [3]. The G-type ordering is the antifer-

Structural parameters obtained in the Rietveld refinement of the NPD pattern with $\lambda = 1.79635$ Å; $Pbnm$ space group

$La_{0.5}Ca_{0.5}MnO_{2.75}$ phase at 250 K*				
Atom	x	y	z	B_{iso}, Å^2 ***
La/Ca (4c)	0.013(8)	0.005(10)	0.25	0.75(36)
Mn (4b)	0	0.5	0	0.97(39)
O1 (4c)	0.049(16)	0.485(16)	0.25	3.55(39)
O2 (8d)	0.734(11)	0.263(13)	0.030(6)	3.55(39)
$La_{0.5}Ca_{0.5}MnO_{2.75}$ phase at 1.6 K**				
Atom	x	y	z	B_{iso}, Å^2
La/Ca (4c)	0.995(13)	0.008(8)	0.25	0.57(35)
Mn (4b)	0	0.5	0	0.78(37)
O1 (4c)	0.054(13)	0.489(13)	0.25	3.12(30)
O2 (8d)	0.733(9)	0.267(9)	0.030(6)	3.12(30)

* Cell parameters are $a = 5.428(4)$ Å, $b = 5.414(5)$ Å, $c = 7.675(6)$ Å; the total number of reflections is 165; the conventional Rietveld R factors are $R_P = 5.72\%$, $R_{WP} = 7.85\%$, $R_{exp} = 3.72\%$; the Bragg R_B is 7.73%; $\chi^2 = 4.77$.
** Cell parameters are $a = 5.421(5)$ Å, $b = 5.406(5)$ Å, $c = 7.664(7)$ Å; the total number of reflections is 165; the conventional Rietveld R factors are $R_P = 6.04\%$, $R_{WP} = 8.07\%$, $R_{exp} = 3.75\%$; the Bragg R_B is 6.73%; $\chi^2 = 4.62$; the magnetic R-factor is 5.60%.
*** B_{iso} is an isotopic temperature factor.

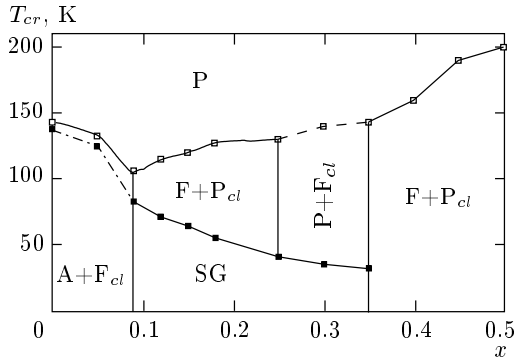

Fig. 6. Magnetic phase diagram of $La_{1-x}Ca_xMnO_{3-x/2}$. A denotes the antiferromagnet with the magnetic structure of the A-type, F_{cl} are ferromagnetic clusters, F + P_{cl} is the inhomogeneous ferromagnet, SG is the spin glass, and P is the paramagnet. The solid line indicates critical temperatures. The dash-and-dot line traced through the full squares is not significant. The dashed line is traced trough $x = 0.30$ because it is a singular point

romagnetic ordering on the nearest-neighbor magnetic sites. Addition of Ca ions destroys the antiferromagnetic order. The ferromagnetic behavior starts to manifest itself at $x \approx 0.1$ and the compositions with x up to 0.3 have both antiferromagnetic and ferromagnetic characteristics. The composition with $x = 0.3$ is clearly ferromagnetic, while the compositions with $x > 0.5$ are antiferromagnetic. In agreement with extensive NMR data [12, 28], the concentration phase transitions go through the mixed two-phase state at the dopant ion values $x < 0.1$ and $x > 0.5$ [29].

The diagram of $La_{1-x}Ca_xMnO_{3-x/2}$ series (Fig. 6) consists of six regions. The concentration boundaries are traced through the critical points. The compositions in the range $0 \le x \le 0.09$ demonstrate a magnetization peak, whereas the spontaneous magnetization gradually increases. We assume that the ground state is antiferromagnetic in this range, probably of the A-type similar to that observed for the parent $LaMnO_3$ composition [3]. The ferromagnetic component could be attributed to the noncollinear magnetic structure or ferromagnetic clusters. It is well known that noncollinear magnetic structure must result from the double exchange between Mn^{3+}/Mn^{4+} ions [6]. However, the $La_{1-x}Ca_xMnO_{3-x/2}$ system does not contain Mn^{3+}/Mn^{4+} pairs. Therefore, the magnetic behavior results from superexchange interactions between Mn^{3+}–O–Mn^{3+}. In this analysis, we assumed that

the ferromagnetic component develops because of ferromagnetic clusters associated with the domains where the static Jahn–Teller distortions are removed. According to Goodenough's considerations [11], the Mn^{3+}–O–Mn^{3+} superexchange magnetic interaction is ferromagnetic and no static Jahn–Teller correlations occur. The removal of the static Jahn–Teller distortions is provided by a small amount of the oxygen vacancies that weakly affect the anion coordination of the majority of the Mn^{3+} ions. Taking all this into account, it seems reasonable to assume that in the range $0 \le x \le 0.09$ our compounds are ferromagnetic clusters in the antiferromagnetic medium. The open squares in Fig. 6 denote the magnetic transition onset temperature. The full squares demonstrate the ZFC-magnetization peak temperature. In the range $0 \le x \le 0.09$, these two temperatures are sufficiently close, and the dash-and-dot line traced through the filled symbols is not significant.

We note that the appearance of the oxygen vacancies stabilizes the other local orbital state in the two nearest Mn^{3+} ions rather than the state in the parent matrix. This process gradually destroys the long-range orbital ordering inherent to $LaMnO_3$, thereby leading to a collapse of the long-range orbital order at $0.09 < x \le 0.35$. However, the pure ferromagnetic ground state does not develop in this region. Magnetization data (Figs. 2 and 3) indicate that the ferromagnetic component is strongly destabilized, which is likely due to a competition between antiferromagnetic and ferromagnetic exchange interactions. We think that the nature of the antiferromagnetic interactions in this region is different from that for the parent $LaMnO_3$. It is well known that $LnMnO_3$ (Ln = Y, Er, Ho, Lu, Sc) with the hexagonal structure are antiferromagnets with T_N around 80 K [30]. In these compounds, the Mn^{3+} ions are located in the 5-fold coordination. For example, magnetic properties of the $La_{0.85}Ca_{0.15}MnO_{2.92}$ composition can be understood assuming that Mn^{3+} (5-fold coordination)–O–Mn^{3+} (5-fold coordination) and Mn^{3+} (5-fold coordination)––O–Mn^{3+} (6-fold coordination) exchange interactions are antiferromagnetic whereas the Mn^{3+} (6-fold coordination)–O–Mn^{3+} (6-fold coordination) exchange interactions are ferromagnetic. For compositions in the range $0.09 < x \le 0.35$, the long-range ferromagnetic ordering is not realized, which is likely due to the increasing oxygen vacancy number above the critical concentration. In this region, the transition in the magnetic ordering state goes through two stages. This can be understood from the ZFC and FC curves. The ZFC magnetization value first starts to increase, reaches its maximum, and then rapidly decreases. The FC magnetization behaves differently. It does not undergo a fall at low temperatures. This magnetization fall may be explained by the magnetic interaction energy between ferromagnetic clusters being insufficient to align their magnetic moments after zero-field cooling. After the field cooling, however, the magnetic moment directions remain the same. This magnetization behavior is typical of the spin glasses where magnetic clusters of magnetic moments are gradually blocked with decreasing temperature. The dashed line is traced trough $x = 0.3$ because it is a singular point, where the spontaneous magnetization is minimal and the temperature coincides with that of the ZFC magnetization peak. It is possible that the magnetic behavior of the compounds in the vicinity of this point has more sharp modifications than those presented in this diagram.

The developing ferromagnetic component in the compositions with the calcium concentration $0.35 < x \le 0.50$ may be the result of a short-range ordering of oxygen vacancies. Apparently, the oxygen vacancies trend to order such that the ferromagnetic part of the exchange interaction between Mn^{3+} placed in the 6-fold coordination becomes more intense than the antiferromagnetic one. In this region, the samples appear to be inhomogeneous ferromagnets. In support of this hypothesis, let us recall several research results. Recently, it was found from high-resolution electron microscopy and selected-area electron diffraction measurements that the stoichiometry $La_{0.5}Ca_{0.5}MnO_3$ and reduced $La_{0.5}Ca_{0.5}MnO_{2.75}$ compounds differ by the domain sizes. The reduced samples have a much smaller domain size and a larger number of domains than the stoichiometry ones. It is therefore reasonable to assume the oxygen vacancies to be accomodated in the domain walls [16].

It is interesting to note that the compositions with $x = 0.15$ and $x = 0.50$ show a relatively large magnetoresistance despite the absence of the mixed valence in manganese. We suppose that the electric conductivity of reduced samples has an impurity nature. There are impurity levels associated with a small number of Mn^{2+} or Mn^{4+} ions. These impurity states are located near the structure defects such as the oxygen vacancies and are probably characterized by very wide energy spectra.

The magnetoresistance may result from a strong decrease of the energy gap between shallow impurity levels and a wide conduction band induced by the external magnetic field applied to the magnetically ordered state.

4. CONCLUSIONS

We can summarize our results as follows.

1. The sign of the Mn^{3+}–O–Mn^{3+} superexchange magnetic interaction depends on the orbital orientation in the orbitally ordered phases of manganites. The magnetic structure can be deduced from the orbital ordering and Goodenough–Kanamori rules [11].

2. Oxygen vacancies remove the orbital ordering in the manganites. This process is in some aspects analogous to the Mn^{4+} doping of $LaMnO_3$ parent compound.

3. In the orbitally disordered phase, the sign of the Mn^{3+}–O–Mn^{3+} superexchange interaction depends on the oxygen neighborhood. When both Mn^{3+} ions are in a six-fold oxygen surrounding, the Mn^{3+}(VI)–O–Mn^{3+}(VI) magnetic interaction is ferromagnetic. In the case where both Mn^{3+} ions or one of them are in a five-fold oxygen surrounding, the Mn^{3+}(V)–O–Mn^{3+}(V) and Mn^{3+}(VI)–O–Mn^{3+}(V) interactions are antiferromagnetic.

4. The system $La_{1-x}Ca_xMnO_{3-x/2}$ with $x \geq 0.35$ is decomposed into clusters with different chemical compositions. The clusters with a high calcium content are ferromagnetic whereas those with a low calcium content are antiferromagnetic.

5. The manganites can exhibit a large magnetoresistance despite the absence of Mn^{3+}–Mn^{4+} pairs. These data support the superexchange picture of magnetic interactions in manganites.

This work was supported in part by Belarus Fund for Fundamental Research (grant F99R-038), Germany Academic Exchange Service (DAAD) and NATO linkage grant (PST.CLG 975703).

REFERENCES

1. S. Jin, T. H. Tiefel, M. McCormack et al., Science **264**, 13 (1994).
2. S. Yunoki, J. Hu, A. L. Malvezzi et al., Phys. Rev. Lett. **80**, 845 (1998).
3. E. O. Wollan and W. C. Koehler, Phys. Rev. **100**, 545 (1955).
4. G. Matsumoto, J. Phys. Soc. Jap. **29**, 606 (1970).
5. C. Zener, Phys. Rev. **82**, 403 (1951).
6. P.-G. De Gennes, Phys. Rev. **118**, 141 (1960).
7. P. W. Anderson and H. Hasagawa, Phys. Rev. **100**, 675 (1955).
8. A. J. Millis, P. B. Littlewood, and B. I. Shraiman, Phys. Rev. Lett. **74**, 5144 (1955).
9. M. A. Subramanian, B. H. Tobi, A. P. Ramirez et al., Science **273**, 81 (1996).
10. I. O. Troyanchuk, D. D. Khalyavin, E. F. Shapovalova et al., Phys. Rev. B **58**, 2422 (1998).
11. J. B. Goodenough, A. Wold, R. J. Arnott, and N. Menyuk, Phys. Rev. **124**, 373 (1961).
12. G. Allodi, R. De Renzi, F. Licci, and M. W. Piepper, Phys. Rev. Lett. **81**, 4736 (1998).
13. I. O. Troyanchuk, D. D. Khalyavin, S. V. Trukhanov et al., Письма в ЖЭТФ **70**, 583 (1999) [JETP Lett. **70**, 590 (1999)].
14. I. O. Troyanchuk, S. V. Trukhanov, H. Szymczak et al., J. Phys.: Condens. Matter **12**, L155 (2000).
15. I. O. Troyanchuk, D. D. Khalyavin, S. V. Trukhanov et al., J. Phys.: Condens. Matter **11**, 8707 (1999).
16. J. M. Gonzalez-Calbet, E. Herrero, N. Rangavittal et al., J. Sol. St. Chem. **148**, 158 (1999).
17. I. Maurin, P. Barboux, Y. Lassailly et al., J. Magn. Magn. Mat. **211**, 139 (2000).
18. B. C. Tofield and W. R. Scott, J. Sol. St. Chem. **100**, 183 (1974).
19. G. Matsumoto, J. Phys. Soc. Jap. **29**, 615 (1970).
20. C. W. Searle and S. T. Wang, Canad. J. Phys. **47**, 2023 (1969).
21. K. Kubo, J. Phys. Soc. Jap. **33**, 21 (1972).
22. K. Kubo, J. Phys. Soc. Jap. **33**, 929 (1972).
23. P. Shiffer, A. P. Ramirez, W. Bao et al., Phys. Rev. Lett. **75**, 3336 (1995).
24. A. Urushibara, Y. Moritomo, T. Arima et al., Phys. Rev. B **51**, 14103 (1995).
25. И. О. Троянчук, ЖЭТФ **102**, 251 (1992) [I. O. Troyanchuk, Sov. Phys. JETP **75**, 132 (1992)].
26. Т. И. Арбузова, И. В. Смоляк, С. В. Наумов и др., ЖЭТФ **116**, 1664 (1999) [T. I. Arbuzova, I. B. Smolyak, S. V. Naumov et al., Sov. Phys. JETP **85**, 899 (1999)].
27. R. D. Shannon, Acta Crystallogr. A **32**, 751 (1976).
28. G. Papavassiliou, M. Fardis, M. Belesi et al., Phys. Rev. B **59**, 6390 (1999).
29. C. N. R. Rao, R. Manesh, A. K. Raychaudhuri et al., J. Phys. Chem. Sol. **59**, 487 (1998).
30. W. C. Koehler, H. L. Yakel, E. O. Wollan et al., Phys. Lett. **9**, 93 (1964).